Solar Energy 259 (2023) 174–187

Contents lists available at ScienceDirect

Solar Energy

journal homepage: www.elsevier.com/locate/solener

Predictability and interrelations of spectral indicators for PV performance in multiple latitudes and climates

M.A. Sevillano-Bendezú [a], M. Khenkin [b], G. Nofuentes [c], J. de la Casa [c], C. Ulbrich [b,*], J.A. Töfflinger [a]

[a] Departamento Académico de Ciencias, Sección Física, Pontificia Universidad Católica del Perú, Av. Universitaria 1801, 15088 Lima, Perú
[b] PVcomB, Helmholtz-Zentrum Berlin für Materialien und Energie GmbH, Schwarzschildstraße 3, 12489 Berlin, Germany
[c] IDEA Research Group. Centre for Advanced Studies in Energy and Environment. University of Jaén, Campus Las Lagunillas, 23071 Jaén, Spain

ARTICLE INFO

Keywords:
Photovoltaic energy yield
Spectral impact prediction
Measured spectral irradiance
Energetic spectral indicators
Spectral Mismatch Factor
Average Photon Energy

ABSTRACT

When PV is installed in the field, the module technologies are rated according to their output energy yield under local operating conditions rather than at standard test conditions (STC), where the spectrum is set to AM1.5G. Care must be taken as this standard is not optimal for all latitudes and the solar spectral distribution variations are one primary influencing factor on PV performance. In addition, obtaining an accurate estimate of the spectral effects on PV performance, as set out in standard procedures, is hampered by the cost of gathering the inputs and the large amount of spectral data required for such a calculation. In this work, based on measured spectral irradiance data from nine sites of different latitudes and climates, we first show a characteristic trend in the spectral distribution over the year concerning the location latitude. The closer a site is to the equator, the more blue-rich the solar spectrum is and the fewer seasonal spectral variations it will contain. Then, we calculate and correlate the most popular metrics (device-independent and device-dependent) used to describe the influence of solar spectra on PV performance. In particular, the monthly irradiance-weighted Spectral Mismatch Factor for different PV technologies and Average Photon Energy show a global linear correlation for data from these nine sites. We use this global linear relationship to propose PV technology-dependent equations that predict annual and monthly spectral gains/losses within a prediction half-interval of up to ± 1.66% by only inserting the monthly or annual irradiance-weighted Average Photon Energy potentially for any site. Reducing the required spectral data sets for performance estimation through our methodology facilitates a more accessible and less costly communication of databases than complete spectral data sets. Finally, using this spectral data, we demonstrate statistically that the Spectral Mismatch Factor and Integrated Useful Fraction Ratio can be replaced by alternative spectral metrics, which require only averaged spectra and, thus, reduce the computational effort to estimate the above indicators.

1. Introduction

Energy production from solar PV is expected to continue its rapid expansion in the coming decades. The installed capacity is estimated to increase to nearly 5,200 GW by 2030 and exceed 14,000 GW by 2050, generally in the form of utility-scale [1]. This increase aims to accelerate the global energy transition, contributing to reducing annual CO_2 emissions to limit temperature rise due to global warming. It is also essential for long-term energy security, price stability, and national resilience, matching some of the goals of the sustainable development agenda [1,2]. To this end, the PV industry must reach a mature market level, guaranteeing investors' confidence and thus fostering PV projects' bankability [3–5]. For instance, the proper selection of PV module technology for PV projects in a specific location can be of the utmost importance for investors and PV project developers, backed by reliable yield estimations in a particular climate [6]. In recent years, yield estimations have shifted focus to rating PV module technologies according to their output energy yield under local operating conditions rather than rating by their power at standard test conditions (STC) [6–10]. Together with the larger effects of irradiance and module temperature variations, the varying solar spectral irradiance is considered an influencing factor on PV module performance.

* Corresponding author.
E-mail address: carolin.ulbrich@helmholtz-berlin.de (C. Ulbrich).

https://doi.org/10.1016/j.solener.2023.04.067
Received 20 December 2022; Received in revised form 26 April 2023; Accepted 30 April 2023
Available online 22 May 2023

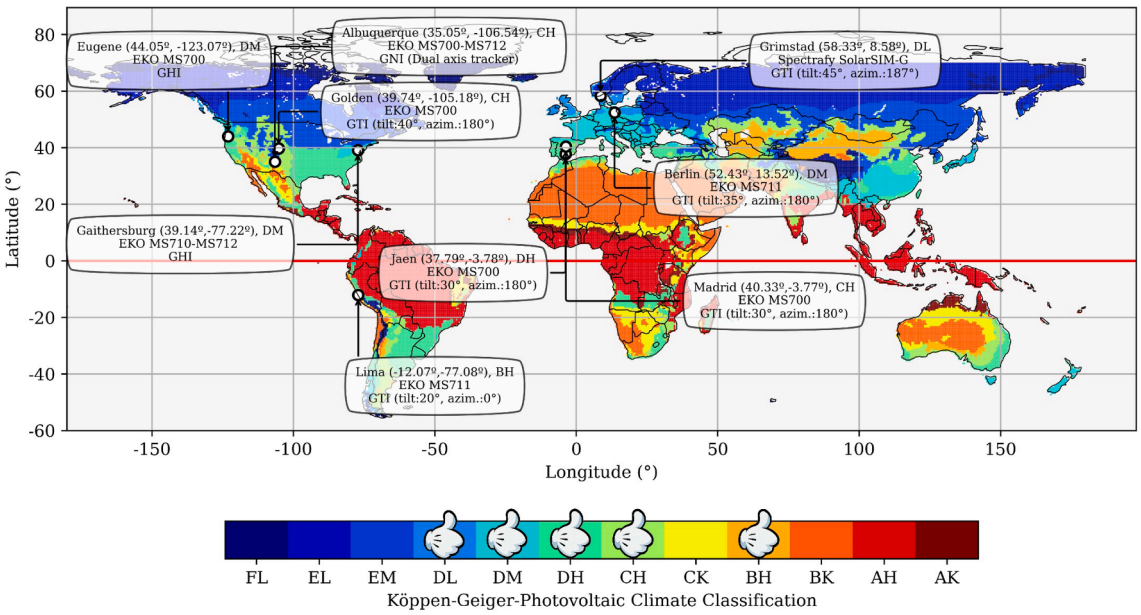

Fig. 1. Köppen-Geiger-Photovoltaic (KGPV) [38] climate classification map with the nine selected sites worldwide, covering 5 of the 12 climate classifications. KGPV Zones are mainly classified according to their temperature-precipitation conditions (first letter) in Tropical (A), Desert (B), Steppe (C), Temperate (D), Cold (E), and Polar (F). The second classification criterion is the irradiation (second letter): Very High (K), High (H), Medium (M), and Low (L) irradiation. We took the open dataset with a spatial resolution of 0.5° × 0.5° from [39]. Dots on the map correspond to the locations where the solar spectral data used in this study was recorded.

Even if the influence is smaller than that of irradiance and temperature, even a small percentage of error in yield estimations during decades of operation has implications in billions of euros in profit or loss [11].

The spectral impact can be evaluated based on measured short circuit current or calculated from solar spectra. Using short circuit current, it is challenging to isolate spectral effects from temperature, soiling, or the influence of the angle of incidence [12,13]. On the other hand, ground-based spectral databases remain scarce, and available spectral data often span over a limited range of wavelengths [14,15]. Synthetic spectra, such as those provided by the National Solar Radiation Database [16–18], offer an alternative for a particular site when spectral data is unavailable [19,20]. However, estimating the spectral impact and a site's spectral characterization from large amounts of data composed of several spectral inputs is impractical to report. Faced with this, representing the solar spectrum by spectral indicators demonstrates a utility by condensing the extended spectral range into a single easily reportable and comparable scalar value [21,22].

The available range of spectral indicators with specific assumptions and associated uncertainties also makes finding general rules harder. Rodrigo et al. (2017) [23] classify spectral indicators into two groups: those independent of the PV device, such as the Average Photon Energy (*APE*, in eV) and those dependent on information from the PV device. Rodrigo et al. (2019) [24] presented a comparative analysis of different spectral indicators based on simulated spectral data from Granada, Spain, to analyze their associated accuracy in predicting spectral impact. They demonstrated that the appropriate choice of spectral indicators for predicting the spectral effects on PV performance depends on the type of PV material studied in Granada. In addition, they pointed out the importance of carrying out a study under different climates worldwide to have a general frame of reference for the different spectral methodologies available, as the present work indirectly aims.

Louwen et al. (2017) [25] showed a scatter plot between different spectral indicators such as the Blue Fraction (*BF*), Useful Fraction (*UF*), the Spectral Mistmatch Factor (*SMM*) vs. the *APE* with experimental spectral irradiance data from Utrecht, the Netherlands. The device-dependent index considered the most accurate to date is the *SMM* [26,27], whose value represents a fraction of the spectral gains or losses in the photocurrent (in comparison to the photocurrent under illumination with AM1.5G spectrum and the same broadband irradiance). Specific experimental conditions and information such as a defined PV technology's spectral response (SR) and a set of wide wavelength range measured spectral irradiances are required to ensure a reliable and accurate calculation, as detailed by Dirnberger et al. (2015) [15]. Ishii et al. (2013) [28] report a polynomial relationship between instantaneous *MM* and *APE* for different photovoltaic technologies from data measured in Kusatsu (Japan). Note that a statistical verification of *APE* uniqueness for specific locations, initially in Kusatsu and extending to other regions in Japan has been shown [21,29]. Chantana et al. (2017) [30] showed a quasi-linear relationship between *SMM* of various PV technologies and *APE* for 71 spectral bands between 350 and 1050 nm in Kusatsu. That work was expanded by Tsuji et al. (2018) [31] for a few more locations, obtaining a more comprehensive range of *APE*.

In addition, the quasi-linear relationship using the same methodology as in [21] and [29] was found when taking different reference devices in calculating the *SMM* [32]. These studies were later extended to other regions of Japan [12,33]. Additionally, Takeguchi et al. (2022) [34] recently presented a set of contour plots to estimate the spectral gain or loss based on an average energetic *APE* and its standard deviation in a gaussian distribution for seven different SRs, using a spectral range from 350 to 1700 nm.

Alternatively, and in parallel, Nofuentes et al. (2014) [35] made a detailed analysis of the relationship between the instantaneous *APE* and an index essentially similar to the *SMM* for Jaen, Spain. One year later, Dirnberger et al. (2015) [14] in Freiburg, Germany, ruled out any bijective relationship between *SMM* and *APE* but also showed the advantage of directly calculating the spectral impact through the monthly weighted *APE* when using the linear regression of these energetic spectral indicators. In the same vein, a study presented by Nofuentes et al. (2017) [36] based on ground-based spectral irradiance data collected over the course of a 2-year experimental campaign conducted in Madrid and Jaen (Spain) disproved the one-to-one relationship between *APE* and the global tilted irradiance (GTI) spectrum shape for these two locations. Recently, Neves et al. (2021) [37] determined linear regressions between monthly weighted *SMM* and *APE* for two locations in Brazil. Although these isolated linear empirical

Table 1
Summary of the characteristics of each installation. Spectral data correspond to GTI, GHI, and GNI. Superscript letters in brackets indicate contributing authors' affiliations; otherwise, the numbers in brackets are the references. We sliced the original spectral range to a maximum of 1050 nm (if recorded in a wider range) to ensure the same pre-processing procedure in all sites. After that, we performed the extrapolations resulting in spectra ranging from 280 to 4000 nm.

Location, Latitude, KGPV climate	Type and tilt angle	Spectral sensor	Original spectral range (nm)	Data collection period	Filter by angle of incidence <
Grimstad 58.33° DL [40,41]	GTI 45°	Spectrafy SolarSIM-G	280 – 4000	Jun-2020 – May-2021	60°
Berlin 52.43° DM [b]	GTI 35°	EKO MS711	300 – 1100	Jun-2019 – May-2020	60°
Albuquerque 35.05° CH [42]	GNI	EKO MS700-MS712	350 – 1700	Jan-2014– Dec-2014	90°
Gaithersburg 39.14° DM [43]	GHI	EKO MS710-MS712	350 – 1100	Jun-2015 – May-2016	90°
Madrid 40.33° CH [c]	GTI 30°	EKO MS700	350 – 1050	Jun-2015 – May-2016	60°
Eugene 44.05° DM [44]	GHI	EKO MS700	335.4 – 1059	Jun-2018 – May-2019	90°
Jaén DH 37.79° [c]	GTI 30°	EKO MS700	350 – 1050	Jun-2016 – May-2017	60°
Golden 39.74° CH [45]	GTI 40°	EKO MS700	343 – 1062.8	Jun-2020 – May-2021	60°
Lima −12.07 BH [a]	GTI 20°	EKO MS711	300 – 1100	Jun-2020 – May-2021	60°

relationships between monthly weighted *SMM* and *APE* have been reported locally, no general linear relationship between both spectral indicators have been reported so far spanning different latitudes and climates on a global scale.

This work takes the focus from a local to a global scale by analyzing measured spectral distributions from various climates and latitudes worldwide. We evaluate the ability of different spectral indicators to estimate the spectral impact on the performance of different PV technologies and analyze the interrelationships between different spectral indicators for two cases of spectral information on the PV device: knowing only the bandgap without spectral sensitivity information and knowing the SR. We analyze the global relationship between the monthly irradiance-weighted *SMM* and *APE* spanning the latitudes and climates of the measurement sites. Aiming towards global applicability, we develop an empirical method for determining the annual (monthly) site-specific spectral impact based on information from the annual (monthly) site-specific *APE*.

2. Methodology

2.1. Experimental data acquisition and pre-processing

We collected experimental ground-based spectral data sets from nine different locations covering a broad range of latitudes, climates, and installation conditions, as depicted in Fig. 1.

These locations, the specific instrument characteristics, and the approximate climate type can be visualized with the help of the Köppen-Geiger-Photovoltaic climate classification map [38], as shown in Fig. 1. Each box in Fig. 1 presents the name of the location, latitude, and longitude, and its approximate KGPV climate classification, the spectroradiometer(s) model, and the orientation plane. Table 1 summarizes additional characteristics of each spectral sensor, including collection period, original spectral range, and equipment. The selected nine locations cover a wide range of the variety of climates concerning the potential PV installations worldwide. Each data set covers precisely one year chosen to have the highest spectral data availability at that site. For most sites, a valid day was considered to have>90% data availability during the hours of sunlight.

Global spectral irradiance is generally measured by spectroradiometer sensors in continuous outdoor exposure across the sky hemisphere. These can be, to name a few, grating spectroradiometers such as the EKO MS-710 and filter-type such as the SolarSIM-G, which measures the spectrum at nine different wavelengths and then reconstructs a spectrum from 280 to 4000 nm from atmospheric models [41,46]. We considered three different configurations of global spectral irradiance measurements: measurements made in a horizontal plane corresponding to Global Horizontal Irradiance (GHI, in W/m^2), measurements in an inclined plane coinciding with a fixed plane-of-array, represented here as Global Tilted Irradiance (GTI, in W/m^2) and an experimental campaign with two-axis sun tracking, corresponding to the Global Normal Irradiance (GNI, in W/m^2).

We first limit all measured spectra to the range between 300 nm and 1050 nm for all sites to maintain equal conditions and apply the same analysis procedure for the different locations, spectroradiometers, and measurement configurations. To enhance the spectral range, we adjusted and applied the extrapolation proposed by Neves et al. (2021) [37] in the ultraviolet region from 280 to 300 or, in a few cases, up to 350 nm, depending on the spectral range of experimental data considered in Table 1. We applied the Martin and Ruiz extrapolation method [47] to extend the range from 1050 to 4000 nm. We validated this last extrapolation using experimentally measured data from 1050 to 1700 nm for GHI, GTI, and GNI spectra. As shown in the supplementary information in Figure S1 and S2, differences between extrapolated and measured spectra are small. Then, Martin and Ruiz extrapolation introduced minor deviations to the integrated irradiance. The extrapolation uncertainties are further reduced when averaging to monthly weighted values. Although, as far as we know, the Martin and Ruiz approach has not yet been validated, this extrapolation method has been used to produce a variety of spectral investigations employing the *SMM* [37,47–51].

Even, Kinsey et al. (2022) [11] suggested substituting the spectrum AM1.5G beyond measurement limits in normalized measured spectra, analyzing spectral effects on PV efficiency.

Additionally, we applied some filtering to maximize the data quality. We discarded spectra with an integrated extrapolated irradiance of fewer than 5 W/m^2 and higher than 1500 W/m^2, thus ruling out extreme over-irradiance events and spurious measurements. In addition, we filtered the GTI data sets by the angle of incidence (AoI) using pythons pvlib [52], discarding data for AoI $> 60°$ as recommended by Dirnberger et al. (2015) [15]. The latter additionally allowed minimizing the influence of larger Air Mass (AM) with predominant diffuse irradiation on the global spectral irradiance. This filter was unnecessary for GNI, while we discarded data for AoI $> 90°$ for GHI to preserve periods of the year in which the AoI is larger than 60°. Finally, when considering the filter of AoI $> 90°$ for GTI, though not shown here, the results did not present significant changes.

2.2. PV technologies

For this study, we chose six representative relative SRs of different PV technologies from Conde et al. (2021) [51], as shown in Fig. 2(a). It is also essential to keep in mind that the additional uncertainties due to the varying SR between PV modules of one type, such as a-Si, CdTe, and c-Si, do not significantly influence the spectral impact. [15]. Temperature-related uncertainties about the spectral impact on PV performance are minor as well [53]. Some technologies with tunable bandgap, such as CIGS or halide perovskites, can present significant differences in SR. We use two different SRs for CIGS, as depicted in Fig. 2 (a), and the most widespread archetypical perovskite composition $CH_3NH_3PbI_3$ with a bandgap of ~ 1.6 eV.

We define the relative EQE as the normalized EQE spectra calculated from relative SR data using the relation $EQE(\lambda) = (hc/q\lambda) \times SR(\lambda)$, h

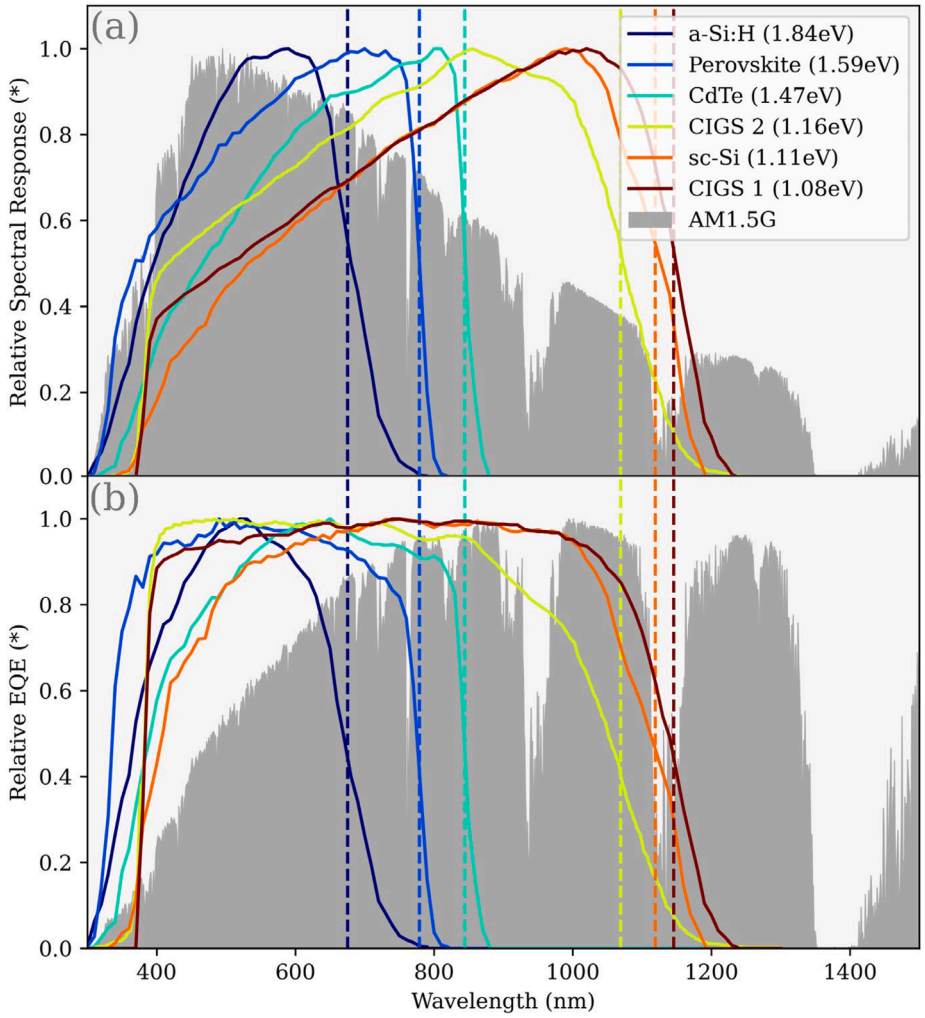

Fig. 2. (a) Relative Spectral response (relative SR) and the normalized spectral irradiance AM1.5G at the background. (b) Relative External Quantum Efficiency (relative EQE) and the normalized photon flux AM1.5G. Dashed lines represent the SQ-Type bandgaps for each PV material calculated according to Rau et al. (2017) [54].

being Planck's constant ($6.62607015 \times 10^{-34}$ m^2kg/s), c the light speed in vacuum (2.9979×10^8 m/s), λ (nm) the wavelength, and q (1.602×10^{-19} C) the elementary electric charge. EQE spectra are a common way to represent the spectral behavior of solar cells. We obtained the bandgaps through the methodology of Rau et al. (2017) [54], which provides a simplified and specific definition of the bandgap, which results from calculating a bandgap that meets the assumptions of the Shockley-Queisser theory [55]. This is called the Shockley-Queisser bandgap (SQ-Type bandgap); from here on, for simplicity, we refer to it as bandgap.

2.3. Spectral indicators

In the following, we present the common figures of merit that quantify the influence of the solar spectrum on PV performance. We present the most common spectral indicators in increasing order of the required inputs. Following Rodrigo et al. (2017) [23], we classify the indexes as PV device-dependent (i.e., they require relative EQE spectrum or device bandgap) and device-independent. To make spectral indicators comparable with previously reported values in the literature, we chose the integration limits accordingly.

The most popular device-independent indicator representing the spectral distribution with a scalar value is the *APE* (in eV) [56,57]. The *APE* is defined as the integrated spectral irradiance of the solar spectrum divided by the integrated photon flux density as shown in Equation (1).

$$APE = \frac{\int_a^b G_{exp}(\lambda)d\lambda}{q\int_a^b \phi_{exp}(\lambda)d\lambda} \quad (1)$$

$$\phi_{exp}(\lambda) = G_{exp}(\lambda)\frac{\lambda}{hc} \quad (2)$$

where $G_{exp}(\lambda)$ (in $Wm^{-2}nm^{-1}$) is the wavelength-dependent measured irradiance, and $\phi_{exp}(\lambda)$ is the associated photon flux density (in $m^{-2}nm^{-1}s^{-1}$) described by Equation (2). We chose the range from $a = 350$ to $b = 1050$ nm. For this considered spectral range, the *APE* for the AM1.5G spectrum ($APE_{AM1.5G}$) is 1.876 eV. Blue-rich spectra translate to values larger than that, and red-rich to smaller values.

Another indicator agnostic of the PV device is the *BF* [22,23]. This index assumes that the blue portion of the spectrum is below 650 nm. Therefore, its definition represents the fraction of blue irradiation described by Equation (3).

$$BF = \frac{\int_a^{650} G_{exp}(\lambda)d\lambda}{\int_a^b G_{exp}(\lambda)d\lambda} \quad (3)$$

The *BF* for the AM1.5 G ($BF_{AM1.5G}$) spectrum is 0.519 in the range from 350 to 1050, which is considered in the present work. A spectrum with a *BF* higher than $BF_{AM1.5G}$ corresponds to a bluer spectrum, a *BF*

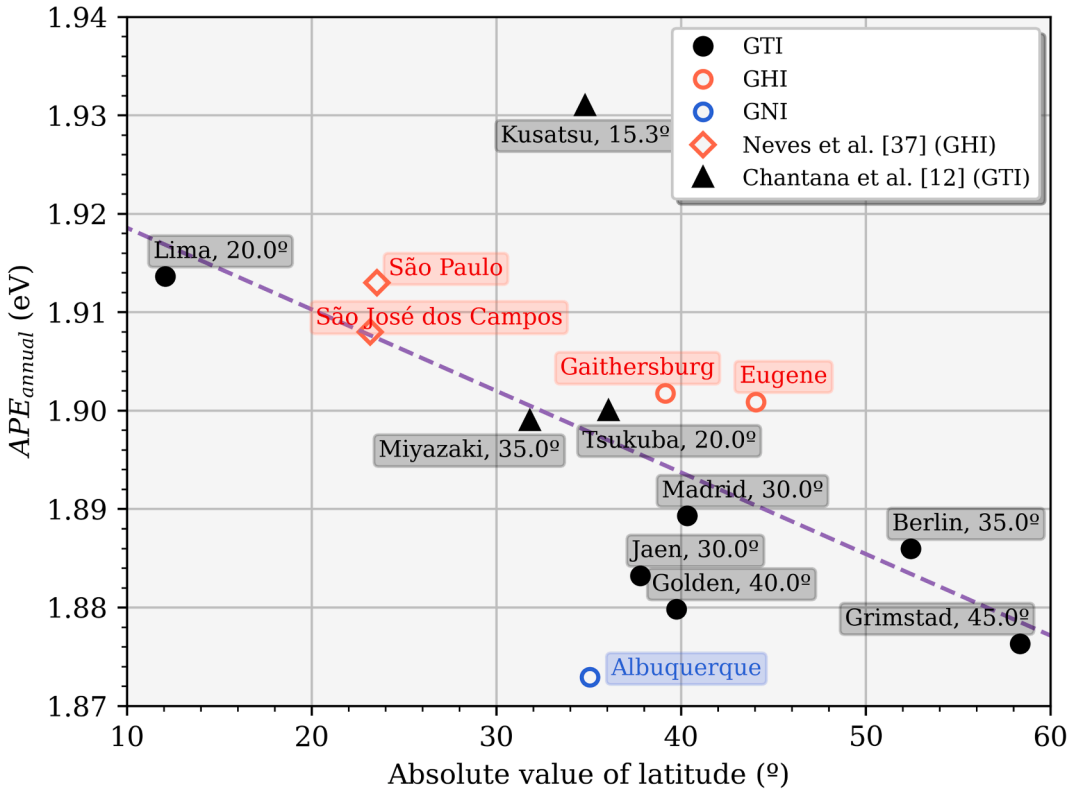

Fig. 3. APE_{annual} as a function of the absolute value of location latitude. We added additional points for São Paulo and São José dos Campos from Neves et al. (2021) [37] and Miyazaki, Kusatsu, and Tsukuba from Chantana et al. (2020) [12]. For GTI data, the spectroradiometer tilt angle is indicated at each location. The dashed line represents the linear fit of all points and indicates the APE_{annual}'s general trend with the absolute value of latitude.

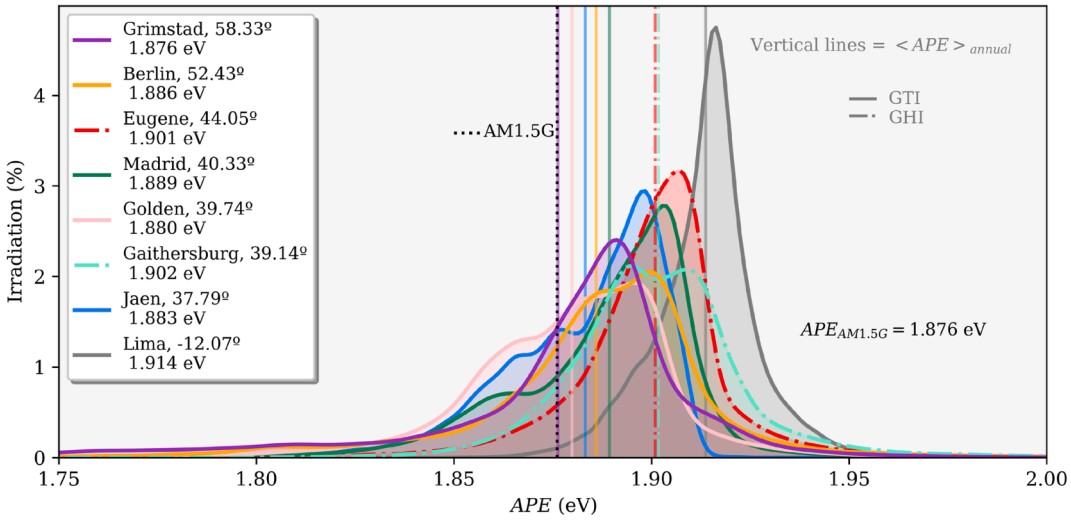

Fig. 4. Irradiation percentage distribution as a function of the *APE* (350–1050 nm) in intervals of 0.001 eV over 12 months at the nine locations obtained by the Kernel Density Estimation (KDE) method. Vertical lines represent APE_{annual}. This Figure does not include the data from the tracked spectroradiometer in Albuquerque.

below $BF_{AM1.5G}$ indicates a red-rich spectrum.

The device-dependent *UF* indicator is defined as the ratio of the irradiance within the spectrally responsive range of the solar cell to the total measured irradiance [58]. The device-dependent index known as the Integrated Useful Fraction Ratio [23] UF/UF^* is the ratio between the *UF* of the measured spectrum and the *UF* of the reference spectrum AM1.5G (UF^*) as shown in Equation (4).

$$\frac{UF}{UF^*} = \frac{\int_c^{\lambda g} G_{exp}(\lambda)d\lambda}{\int_c^{\lambda g} G_{ref}(\lambda)d\lambda} \frac{\int_c^{d} G_{ref}(\lambda)d\lambda}{\int_c^{d} G_{exp}(\lambda)d\lambda} \tag{4}$$

where λg is the wavelength corresponding to the bandgap. $G_{ref}(\lambda)$ ($Wm^{-2}nm^{-1}$) represents the AM1.5G spectrum, and c and d are 280 and 4000 nm, respectively, in the present work.

As mentioned in the introduction section, one of the most representative and widespread indices of spectral impact is the Spectral Mismatch Factor (*SMM*). The IEC 60904–7 standard [18] defines it as

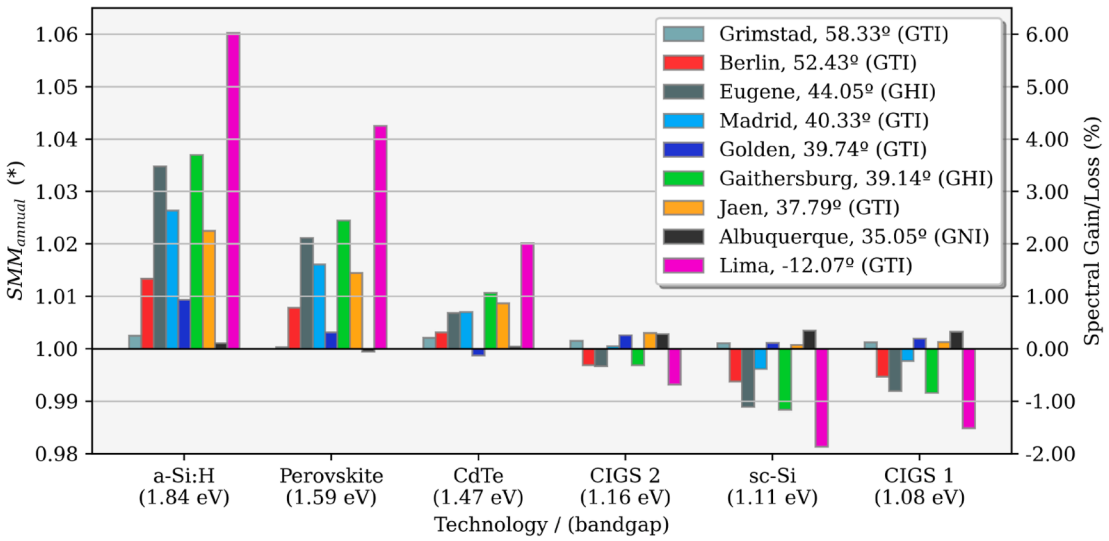

Fig. 5. SMM_{annual} in nine locations for different PV technologies with their respective bandgap in parenthesis. The bars also indicate spectral gains/losses.

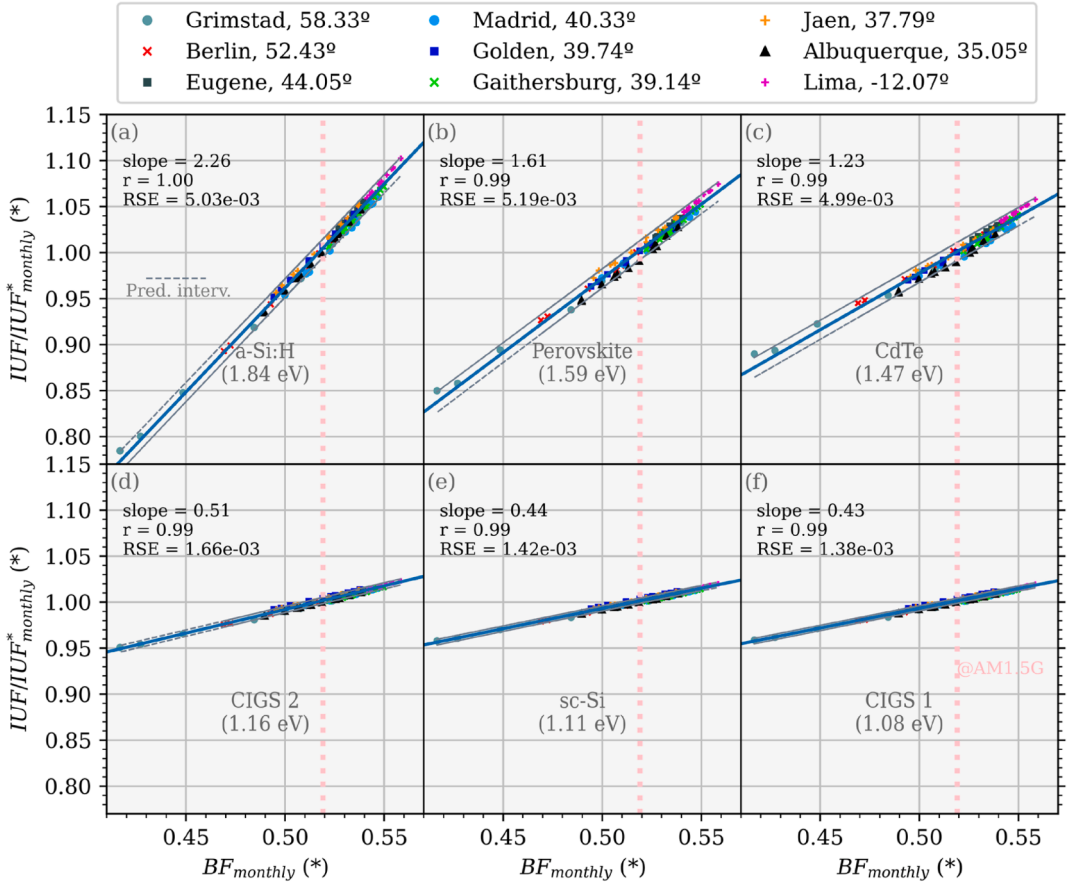

Fig. 6. Linear relationship between $IUF/IUF^{*}_{monthly}$ and $BF_{monthly}$ for six different PV technologies: (a) a-Si: H, (B) Perovskite, (c) CdTe, (d) CIGS 2, (f) sc-Si and (g) CIGS 1. The grey dashed lines indicate the prediction interval. The vertical dotted line indicates *BF* for the AM1.5G spectrum. RSE and r are the residual standard error and the correlation coefficient, respectively.

shown in Equation (5). We choose the range from 280 to 4000 nm to consider the broadest range of the solar spectrum.

$$SMM = \frac{\int_c^d \mathrm{SR}(\lambda)G_{exp}(\lambda)d\lambda \int_c^d G_{ref}(\lambda)d\lambda}{\int_c^d \mathrm{SR}(\lambda)G_{ref}(\lambda)d\lambda \int_c^d G_{exp}(\lambda)d\lambda} \quad (5)$$

This device-dependent index represents an increase or decrease in a PV device's short-circuit current produced by a specific broadband irradiance distributed conforming to an actual spectrum relative to that produced by the same broadband irradiance distributed conforming to the AM1.5G standard. Hence, *SMM* above/below one indicates a spectral gain/loss.

Since this study focuses on energy yield, we convert our instanta-

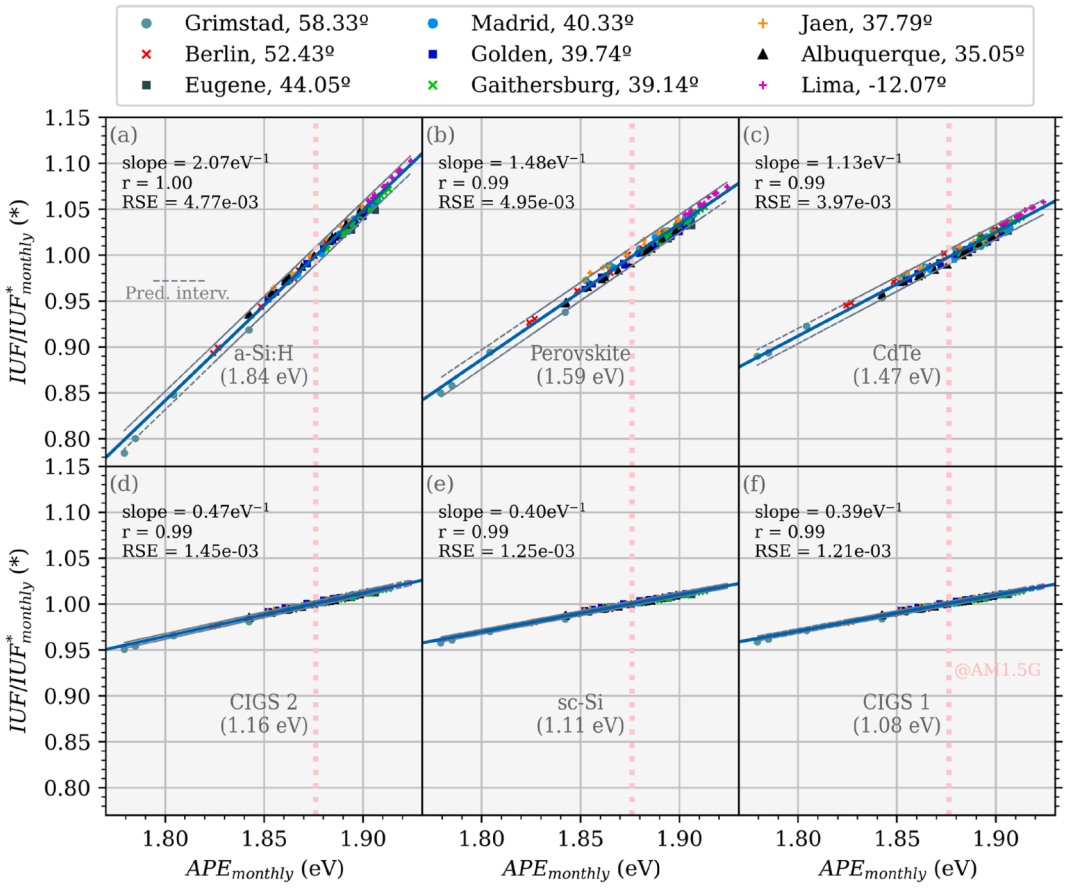

Fig. 7. Linear relationship between $IUF/IUF^{*}_{monthly}$ and $APE_{monthly}$ for six different PV technologies: (a) a-Si: H, (B) Perovskite, (c) CdTe, (d) CIGS 2, (f) sc-Si, (g) CIGS 1. The grey dashed lines indicate the prediction interval. The vertical dotted line indicates *APE* for the AM1.5G spectrum. RSE and r are the residual standard error and the correlation coefficient, respectively.

neous calculated indicators to irradiance-weighted average indicators using Equation (6).

$$< KPI >_T = \frac{\sum_{i=1}^{N_T} KPI_i \times G_i}{\sum_{i=1}^{N_T} G_i} \tag{6}$$

where *KPI* is a Key Performance Indicator that represents our instantaneous spectral indicator, such as the *APE*, *BF*, UF/UF^{*} and *SMM*. G_i (W/m^2) is the *i*-th recorded value of the integrated *i*-th spectral irradiance, $G_{exp}(\lambda)_i$, associated with the *i*-th spectral indicator, *T* (day, month, year) is the period considered (such as daily, monthly or annual) and N_T represents the respective number of measurements along *T*. Note that the so-called Integrated Useful Fraction Ratio (IUF/IUF^{*}) [58] corresponds to the weighted average irradiance (using Equation (6)) of the UF/UF^{*}. A UF/UF^{*} higher than one means that the measured spectrum has a higher fraction of useful irradiance than the reference spectrum. Note that the useful fraction is inaccurate as it overestimates the amount of irradiance absorbed by the device as it uses a step function for the SR instead of the device's SR [24].

Additionally, we adapt two spectral indicators proposed in Rodrigo et al., 2019 [24]. Our adaptation focuses solely on calculating the weighted irradiance spectrum as described by Equation (7), thus reducing the computational effort of calculating additional averages and integrals. We consider the same spectral range ($c = 280$ and $d = 4000$ nm) as the abovementioned indicators.

$$< G_{exp} > (\lambda) = \frac{\sum_{i=1}^{N_T} G_{exp}(\lambda)_i \times G_i}{\sum_{i=1}^{N_T} G_i} \tag{7}$$

The first index refers to the adapted Spectral Average Useful Fraction (for simplicity, we keep the notation *SAUF*), which presents the same expression as IUF/IUF^{*} changing the measured instantaneous spectrum $G_{exp}(\lambda)$ by the $< G_{exp} > (\lambda)$ as represented in Equation (8).

$$SAUF = \frac{\int_c^{\lambda g} < G_{exp} > (\lambda) d\lambda}{\int_c^{\lambda g} G_{ref}(\lambda) d\lambda} \frac{\int_c^{d} G_{ref}(\lambda) d\lambda}{\int_c^{d} < G_{exp} > (\lambda) d\lambda} \tag{8}$$

The second index is called the adapted Spectral Enhancement Factor (for simplicity, we also keep the notation *SEF*) and has the same expression as the *SMM*, except replacing $G_{exp}(\lambda)$ with the $< G_{exp} > (\lambda)$ as expressed in Equation (9).

$$SEF = \frac{\int_c^{d} \mathrm{SR}(\lambda) \langle G_{exp} > (\lambda) d\lambda}{\int_c^{d} \mathrm{SR}(\lambda) G_{ref}(\lambda) d\lambda} \frac{\int_c^{d} G_{ref}(\lambda) d\lambda}{\int_c^{d} < G_{exp} > (\lambda) d\lambda} \tag{9}$$

3. Results and analysis

3.1. Spectral distribution variability and spectral impact assessment in the selected sites.

In general, there is a trend for APE_{annual} to decrease as the distance from the equator increases, as indicated by the dashed linear regression line in Fig. 3. Additionally, to our measured data, we added values reported in previous studies to broaden the range of locations further. We notice that the higher-latitude sites with measured spectral GHI, Gaithersburg and Eugene, exhibit a slightly higher value of APE_{annual}, i.e., spectra shifted to shorter wavelengths. Indeed, spectroradiometers in horizontal position located outside the tropics measure a higher content of blue light during principal daytime hours than if tilted to maximize

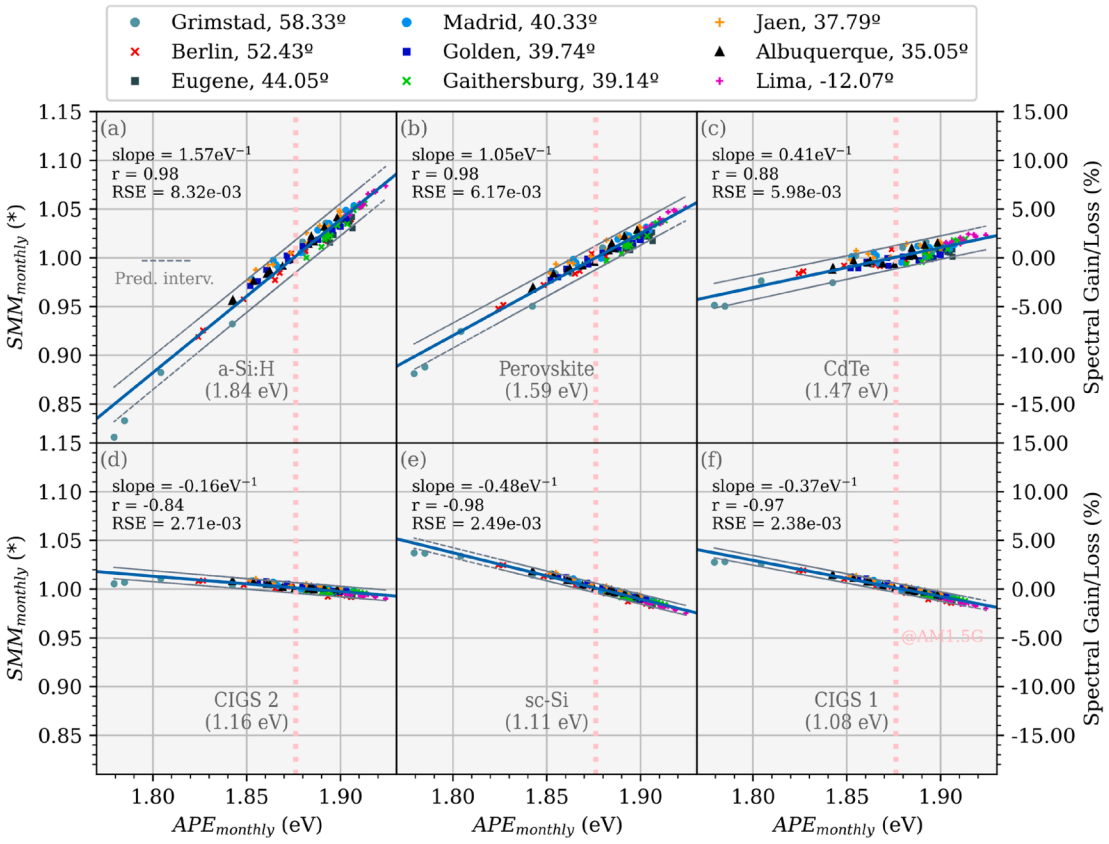

Fig. 8. Linear relationship between $SMM_{monthly}$ (and spectral gains/losses) and $APE_{monthly}$ for six different PV technologies: (a) a-Si: H, (B) Perovskite, (c) CdTe, (d) CIGS 2, (f) sc-Si and (g) CIGS 1. The grey dashed lines indicate the prediction interval. The vertical dotted line indicates *APE* for the AM1.5G spectrum. RSE and r are the residual standard error and the correlation coefficient, respectively.

Table 2
List of empirical equations of the global linear regressions between $SMM_{monthly}$ and $APE_{monthly}$. These equations can be used to calculate *SMM* using *APE* on a monthly and annual basis, potentially, for any location in the world. In addition, we show the approximate half-interval of the prediction interval calculated by assuming the prediction interval as a parallel line.

PV Technology (Bandgap in eV)	Linear Regression equation for *SMM*	Half- prediction interval (10^{-2})	RSE (10^{-3})	r
a-Si (1.84)	$1.5707eV^{-1} \times APE - 1.9452$	1.66	8.3	0.9808
Perovskite (1.59)	$1.0497eV^{-1} \times APE - 0.9692$	1.23	6.2	0.9765
CdTe (1.47)	$0.4102eV^{-1} \times APE + 0.2311$	1.20	6.0	0.8771
CIGS 2 (1.16)	$-0.1580\,eV^{-1} \times APE + 1.2977$	0.54	2.7	−0.8406
sc- Si (1.11)	$-0.4755\,eV^{-1} \times APE + 1.8933$	0.50	2.5	−0.9812
CIGS 1 (1.08)	$-0.3710\,eV^{-1} \times APE + 1.6973$	0.48	2.4	−0.9722

annual irradiation collection. On the contrary, the sun-tracked spectroradiometer in Albuquerque sees less blue sky due to the higher red-light content of GNI compared to that of GTI. Other specific climatic conditions such as cloud cover, aerosols, humidity CO_2, ozone, and the surrounding albedo, not studied here, contribute to the spectral distribution variability in each location. Kusatsu, for instance, exhibits the highest GTI-associated APE_{annual}, even higher than the GHI spectra in the other sites. Several studies refer to Kusatsu as a place with a particularly blue-rich spectral distribution [59,60]. This could be a result of a cloudy climate [61]. This factor apparently outweighs the influence of AM (and hence the latitude) at this location.

Fig. 4 displays the percentage irradiation distribution for the annual data sets. Note that all spectra cover a wide range of *APE* s, which gives statistical significance to the results discussed below. As described in Section 3, we filtered GTI by the AoI to discard spectra with AoI above 60°, so that evening and morning hours with red-rich spectra in GTI were removed from consideration in this paper. All distributions in Fig. 4 show an asymmetry resulting in *APE* values at their maximum that differ from APE_{annual}. In Gaithersburg, two maximums correspond to two different *APE* distributions, one below and the other one above its APE_{annual}. The different degrees of skewness of the distributions originate from the seasonal variations of *APE* of each location, as can be understood from Figure S3 in the supplementary information. Figure S3 shows the seasonal behavior of the *APE* for the six sites with GTI spectral data on different timescales: instantaneous, daily-, weekly-, monthly-, and annual-weighted. It helps to understand, for instance, that the nearly symmetric distribution of the *APE* values in Lima (Fig. 4) originates from the minor variabilities in Lima's *APE* values throughout the year. Additionally, the $APE_{monthly}$ variation throughout the year in Figure S3, i.e., the seasonal spectrum variation of GTI, increases when the latitude and the corresponding traveled AM for the selected sites increase. Accordingly, Grimstad shows the most significant seasonal variation in spectral distribution throughout the year.

Fig. 5 shows the annual *SMM* and the corresponding annual spectral gains and losses (*spectral Gain/Loss* defined as $100\%*(SMM-1)$) for six selected PV technologies. Qualitatively, some reported spectral gain and loss trends [6] for the abovementioned devices are notably verified in four sites: Lima, Gaithersburg, Eugene, and Madrid. The AM1.5G

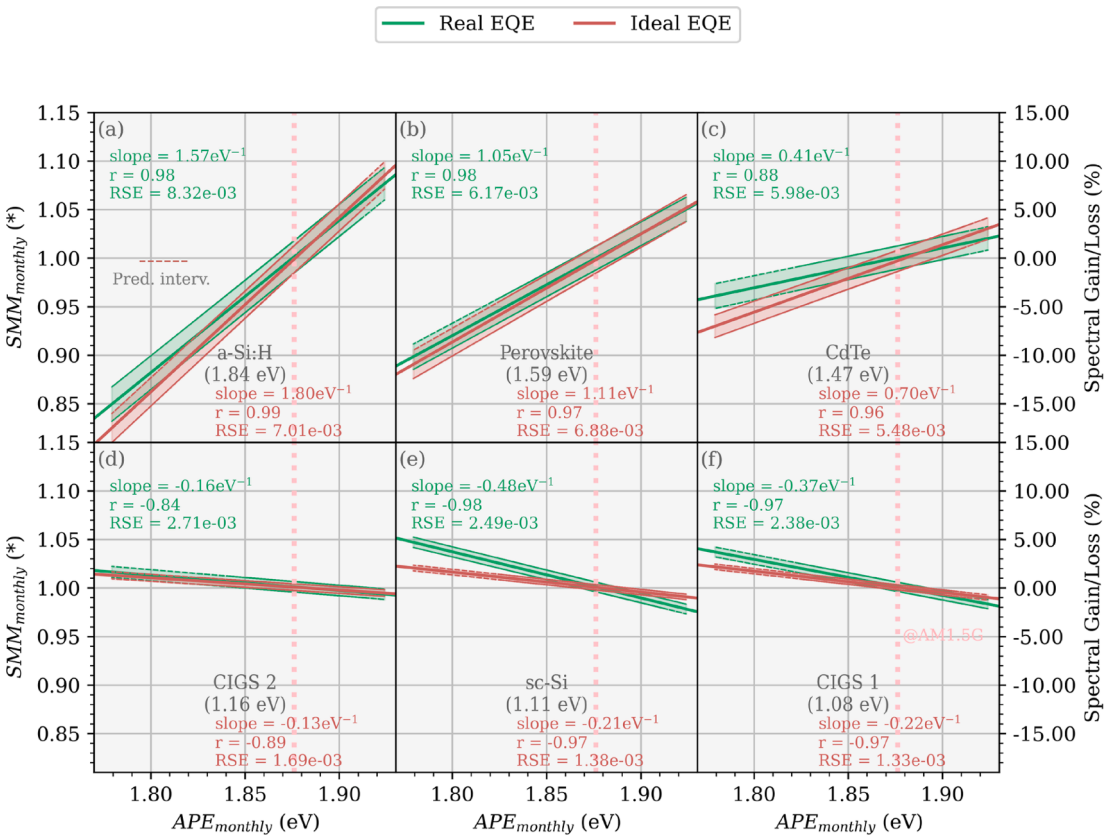

Fig. 9. Comparison of $SMM_{monthly}$ vs $APE_{monthly}$ linear regressions for real (Fig. 2.) and ideal EQEs (step-function EQEs) for six different PV technologies. The shaded area indicates the prediction interval. The vertical dotted line indicates *APE* for the AM1.5G spectrum. RSE and r are the residual standard error and the correlation coefficient, respectively.

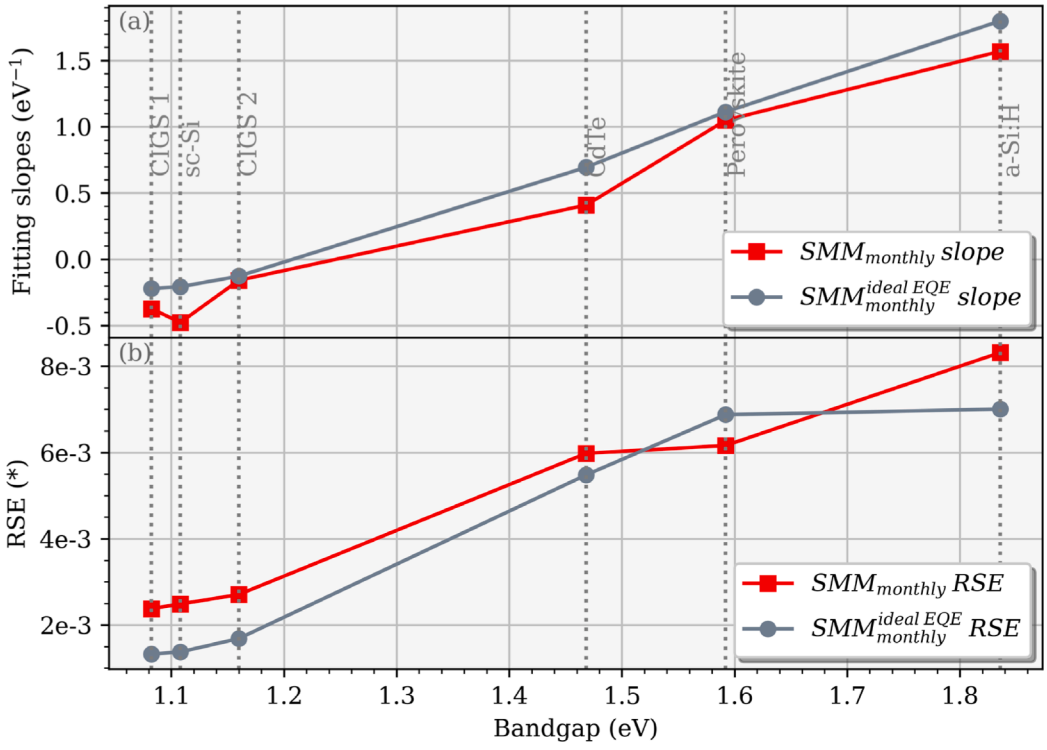

Fig. 10. Comparison in (a) slopes and (b) residual standard error (RSE) vs. PV materials' bandgaps from the $SMM_{monthly}^{idealEQE.}$ and $SMM_{monthly}$ with $APE_{monthly}$ linear regressions.

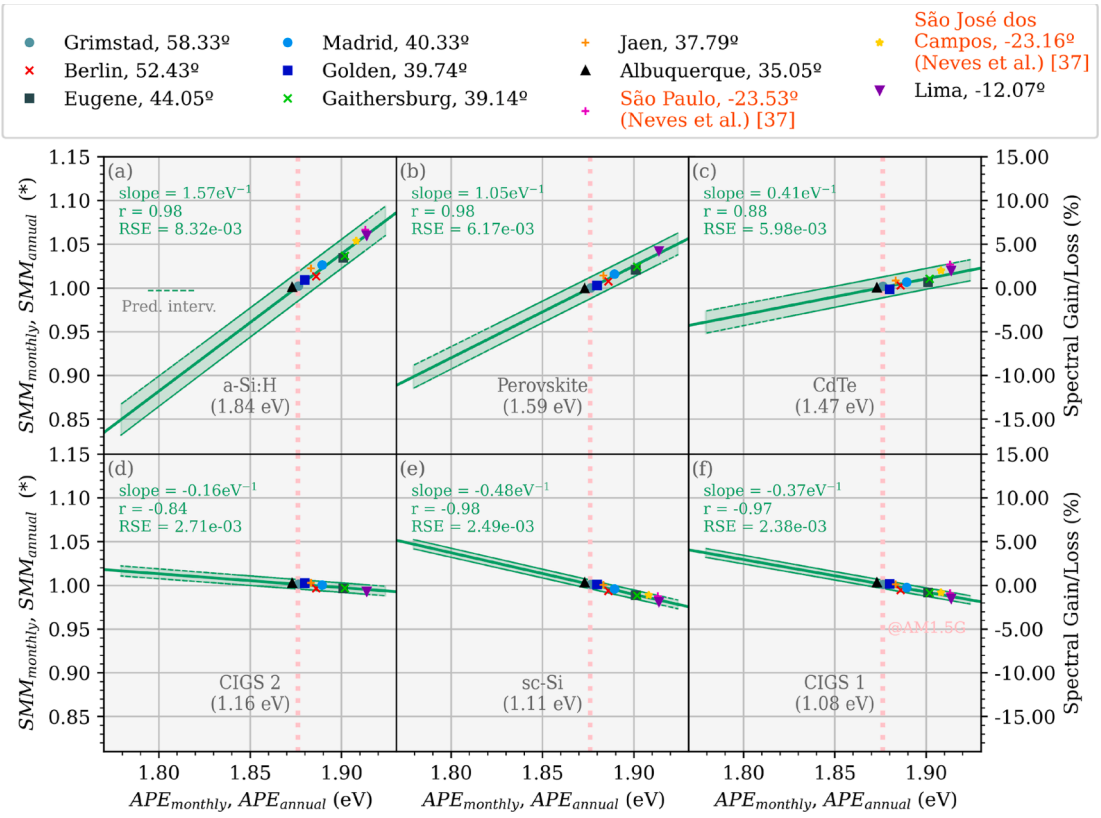

Fig. 11. SMM_{annual} vs APE_{annual} scatter plot on the $SMM_{monthly}$ vs $APE_{monthly}$ linear regression. The annual values are within the monthly weighted linear regression prediction interval. The shaded area indicates the prediction interval. The vertical dotted line indicates *APE* for the AM1.5G spectrum. RSE and r are the residual standard error and the correlation coefficient, respectively.

Table 3
Spectral impact prediction sensitivity by using the equations from Table 2 to predict SMM_{annual}, shown in Fig. 11.

	a-Si:H	Perovskite	CdTe	CIGS 2	sc-Si	CIGS 1
RMSE (10^{-3})	4.79	3.46	2.92	1.77	1.70	1.77
MBE (10^{-4})	6.76	3.96	2.69	1.63	1.54	1.35

reference represents an atmospheric condition predominantly found on mid-latitude sites. Thus, it is unsurprising that the highest magnitude of spectral gains/losses for all the PV technologies was observed in Lima, where this condition fits the least. The annual *APE* in this location is the highest, and the solar spectrum is blue-rich compared to the other locations' distributions and the reference itself throughout the year. In Lima, there are almost no seasons. However, Fig. 5 shows – as was to be anticipated based on the spectral variation distributions in Fig. 4, that just the location latitude is not sufficient to forecast spectral effects on PV performance, since no trend is evident between latitude and spectral gains/losses.

3.2. Interrelations between spectral indicators in order of input required

Fig. 6 shows the relationship between $IUF/IUF^{*}_{monthly}$ and $BF_{monthly}$ for the nine sites and six PV devices represented by their bandgaps. The dashed line marks the 95% prediction interval [62,63]. There is a strong correlation for all technologies with $r \geq 0.99$. Below we propose three hypotheses that would support such a linear relationship:

1. As described in the supplementary information (Supplementary note 1), the mathematical expressions for UF/UF^{*} and *BF* are proportional if not considering the limits of integration.
2. The extrapolation method of Martin and Ruiz (1999) [47] assumes that the irradiance in the band above 1100 nm is proportional to the irradiance of the band from 700 to 1100 nm. Figure S1 shows that the latter assumption is valid in the range from 700 to 1050 nm since the integrated irradiance from 1050 to 1700 nm of the extrapolated spectrum by the Martin and Ruiz method is very similar to the measured irradiance in the same range. Hence, the spectral irradiance could be proportional in different spectral bands. The UF/UF^{*} with the *BF*, considering their integration limits, could present such a proportionality, especially for spectra in clear sky conditions. Consequently, the choice of integration limits would not break the linear relationship between these two spectral indicators.
3. The calculation of the weighted average spectral indicators gives greater weight to the spectra recorded at higher irradiance. Therefore, spectral measurements under clear sky conditions have higher contributions to the metrics UF/UF^{*} and *BF*. This results in avoiding branching of the linear trend, sometimes observed for instantaneous values between similar metrics as in [14].

The RSE of the linear regressions for narrow bandgap technologies is lower by a factor of 3 to 4 compared to solar cells with wide bandgap, as variations in the spectra are expected in the high energy range.

Note the global linear relationship for the $IUF/IUF^{*}_{monthly}$ with the $APE_{monthly}$, as shown in Fig. 7. Interestingly, the linear relationship has RSEs even lower than those obtained comparing $IUF/IUF^{*}_{monthly}$ vs. $BF_{monthly}$. This linearity is very convenient to predict $IUF/IUF^{*}_{monthly}$. $APE_{monthly}$ is an index that is often reported to quantify spectral distributions. Additionally, as shown in Figure S4, the linear relationship remains well justified ($r \geq 0.98$) even if monthly weighted integration is replaced with daily weighted integration.

The *SMM* is one of the most frequently used spectral indicators for

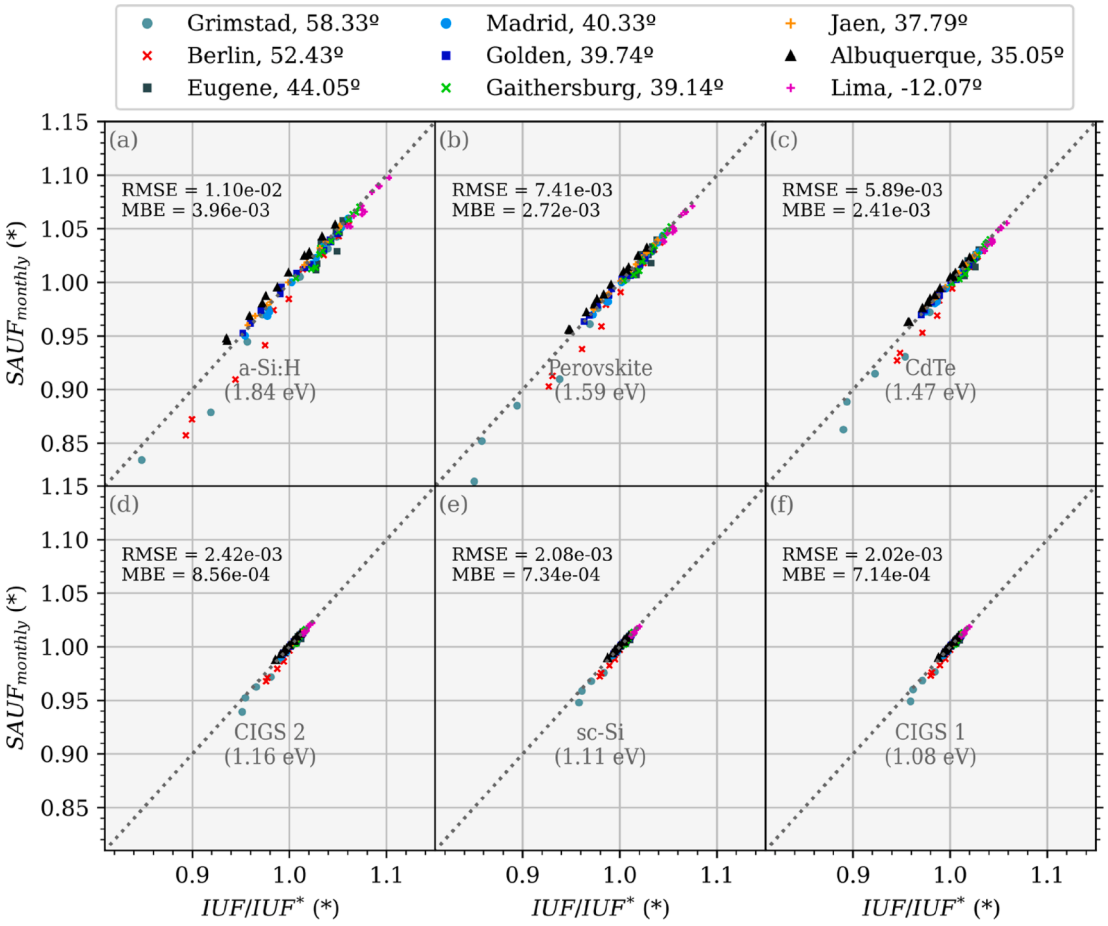

Fig. 12. Comparison between the two bandgap-dependent indicators: $SAUF_{monthly}$ and $IUF/IUF^{*}_{monthly}$ for six different PV technologies, using experimental data from 9 locations. The dashed line represents the identity $SAUF_{monthly} = IUF/IUF^{*}_{monthly}$. RMSE and MBE are the Root Mean Square Error and the Mean Bias Error, respectively.

energy yield calculations due to its intuitive interpretation. However, it is sensitive to different influencing factors that may introduce uncertainties [15]. For instance, an important point is the lack of available wavelength range in the instruments from which spectral measurements are taken. This work uses spectral irradiance from 280 to 4000 nm to reduce that uncertainty.

As reported in the introduction section, the *SMM* and *APE* (monthly weighted) demonstrated a linear relationship in prior studies when analyzed at a particular location. In Fig. 8, we show that the linearity between $SMM_{monthly}$ and the $APE_{monthly}$ is indeed global (see Figure S5 for the daily weighted values). Again, the RSE increases for wider bandgap PV technologies. We summarize the equations resulting from the global linear regressions in Table 2, where we added the estimate of the half-interval of the prediction interval by fitting the prediction interval with parallel lines to the $SMM_{monthly}$ and the $APE_{monthly}$ linear regression. This value expressed in percentage ($\times$ 100%) indicates the half-interval in terms of energy gains and losses.

Comparing Fig. 8 with Fig. 7, we note that IUF/IUF^{*} distorts the trend in spectral gains and losses for CIGS and sc-Si technologies reported in the present work. As expected, IUF/IUF^{*} by itself does not adequately represent spectral effects. By definition, this indicator uses a unitary SR which translates into a hyperbolically shaped EQE [64], vastly different from the typical PV device EQE.

We list three reasons that influence the linearity between $SMM_{monthly}$ and $APE_{monthly}$ in the ideal case (the EQE being a step function, see supplementary note 1 and Figure S6), despite the different integration ranges:

1. SMM_{ideal} and *APE* are proportional as indefinite integrals.
2. The relationship between the integration of different parts of the spectrum is linear, similar to the observation for $IUF/IUF^{*}_{monthly}$ and $BF_{monthly}$. In addition, Kataoka et al. (2014) [29] showed that the *APE* for different integration ranges such as the bands 450–500 nm with 800–850 nm can preserve linearity with the *APE* in the range of 350 to 1050 nm. This observation could contribute to this hypothesis.
3. Same as for $IUF/IUF^{*}_{monthly}$ and $BF_{monthly}$, the linear relationship is supported by irradiance-weighting the $SMM_{monthly}$ and $APE_{monthly}$.

Finally, a measured relative EQE in calculating *SMM* increases the linear relationship dispersion depending on the losses of the experimental relative EQE compared to the ideal solar cell.

Fig. 9 compares linear regressions for ideal (red) and realistic (green) relative EQEs. For high-bandgap absorbers (a-Si:H, perovskite, CdTe), realistic devices show lower slopes than ideal ones, which means lower sensitivity of $SMM_{monthly}$ towards $APE_{monthly}$ changes. On the other hand, low-bandgap devices exhibit negative slopes that are more significant for realistic devices than ideal ones. This indicates a more considerable sensitivity of the $SMM_{monthly}$ towards $APE_{monthly}$ changes for realistic devices. For all devices we observe that the $SMM_{monthly}$ for realistic devices is larger than for ideal ones for $APE_{monthly}$ values below $APE_{AM1.5G}$. This may indicate, that realistic devices exhibit more significant relative EQE losses in the lower wavelengths than in larger wavelengths, consequently enhancing $SMM_{monthly}$ for smaller $APE_{monthly}$, and diminishing it for larger $APE_{monthly}$.

Furthermore, the change of the slopes when going from higher to lower bandgap indicates that there possibly exists a device with a

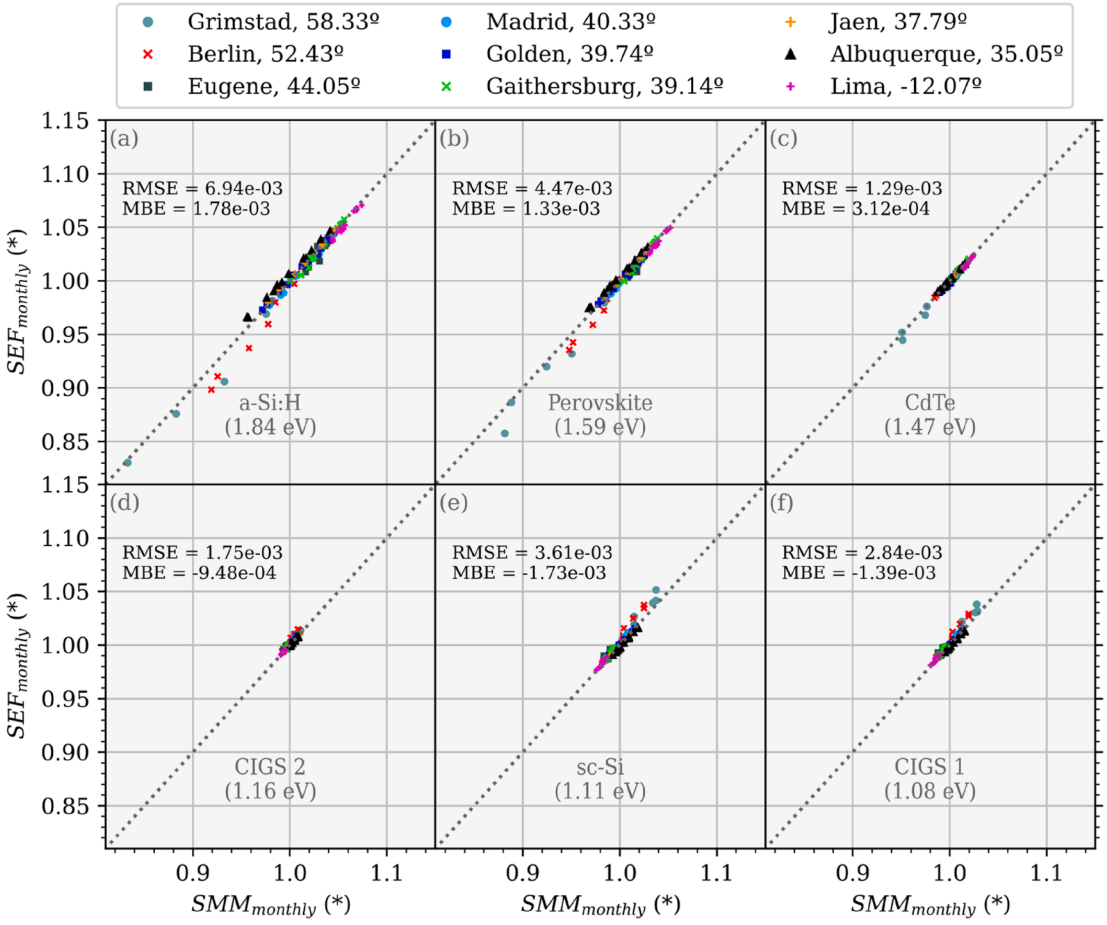

Fig. 13. Comparison between the two EQE-dependent KPIs: $SEF_{monthly}$ and $SMM_{monthly}$ for six different PV technologies, using experimental data from 9 locations. The dashed line represents the identity $SEF_{monthly} = SMM_{monthly}$. RMSE and MBE are the Root Mean Square Error and the Mean Bias Error, respectively.

bandgap and EQE that results in a constant $SMM_{monthly}$, independent of $APE_{monthly}$. The CIGS 2, which demonstrates the lowest slope, approximates to such a device that would be insensitive to spectral changes.

In Fig. 10, we compare the slopes and RSE as functions of the bandgap energy for the monthly *SMM* and *APE* linear regressions with an ideal ($SMM^{idealEQE.}_{monthly}$) and realistic EQE. In Fig. 10(a), we notice a threshold value around 1.2 eV in the case of an ideal EQE, for which, above 1.2 eV, the slopes increase positively while below 1.2 eV the negative slopes decrease as the bandgap increases. In addition, slopes associated with real relative EQE of c-Si and CdTe exhibit a more significant deviation from the ideal ones. However, in Fig. 9, the wide prediction interval for CdTe decreases the gap between the results based on theoretical and measured relative EQE. In contrast, the narrow range of the c-Si prediction interval increases the difference between the results for an actual and an ideal case when trying to predict the spectral impact.

On the other hand, Fig. 10(b) shows the increasing RSE as the bandgap energy increases for the ideal cases. We further note that these RSEs underestimate the RSEs for realistic relative EQEs except for Perovskite, where the ideal RSE overestimates the RSE for measured relative EQE.

In Fig. 11, we have superimposed a scatter plot of the SMM_{annual} versus APE_{annual} with the limits of the calculated prediction intervals of the monthly weighted linear regression. Good agreement with the linear trend and the fact that they are all within the prediction interval confirms our ability to predict the spectral effects using only APE_{annual} and the equations in Table 2. Additionally, as a test, we evaluate the predictive capability of the SMM_{annual} for São Paulo and São Jose dos Campos based on their APE_{annual} reported in Neves et al. (2021) [37]. We also show that the prediction intervals of our general monthly weighted linear relationship harbor those reported values. Table 3 summarizes the prediction sensitivity through the RMSE and the MBE.

Finally, we evaluate the suitability in predicting the IUF/IUF^{*} and irradiance weighted *MM* of two additional spectral energy indicators, *SAUF* and *SEF*, respectively. Both require the calculation of an average solar spectrum instead of the instantaneous spectra as indicated in Equation (7) (see Figure S7 for observing the average monthly weighted spectra in the nine locations), saving computational time. However, to make $SAUF_{monthly}$ and $SEF_{monthly}$ interchangeable with $IUF/IUF^{*}{}_{monthly}$ and $SMM_{monthly}$, respectively, requires careful attention to the associated uncertainties that arise from calculating these two additional indicators, which is outside this work's scope. Rodrigo et al. (2019) [24] analyze these last two indicators using synthetic spectra. However, in this work, we show their direct comparison with their respective associated indicators based on measured spectral data for different latitudes and climates.

Fig. 12 shows the relationship between the $SAUF_{monthly}$ and the $IUF/IUF^{*}{}_{monthly}$. The RMSE is comparable to the $IUF/IUF^{*}{}_{monthly}$'s RSE in its linear relationship with the $APE_{monthly}$ (Fig. 7) and, both indices show similar trends for all technologies. Additionally, positive MBE indicates that the $SAUF_{monthly}$ generally slightly overestimates the $IUF/IUF^{*}{}_{monthly}$ values for all cases.

Similarly, Fig. 13 shows the relationship between $SEF_{monthly}$ and $SMM_{monthly}$. In this case, the RMSE values are lower than the RSE indicated in Fig. 8, except for sc-Si and CIGS 1. While the positive MBE expresses that the $SEF_{monthly}$ generally overestimates the $SMM_{monthly}$ for

wider bandgaps, the opposite occurs for narrow bandgaps. These results show that the $SEF_{monthly}$ provides a reasonable estimation of the $SMM_{monthly}$.

4. Conclusions

We analyzed the interrelationships between different spectral indicators based on ground-based spectral GTI, GHI, and GNI data from nine sites worldwide. We studied latitude as an implicit variable of the spectral distribution and observed a general decreasing trend of the APE_{annual} as the absolute value of latitude increases. Due to the impact of the latitude on the seasonal AM variation, higher seasonal spectrum variation in GTIs was observed in locations further away from the equator. We reviewed the general relationship between the $IUF/IUF^{*}{}_{monthly}$ and the $BF_{monthly}$. These two indicators exhibit a linear relationship. The $IUF/IUF^{*}{}_{monthly}$ is also linear to the $APE_{monthly}$ with even a lower RSE than for the linearity to $BF_{monthly}$.

As the main contribution of this paper, we demonstrate a linear relationship between $SMM_{monthly}$ and $APE_{monthly}$ considering global spectral data from the nine sites. This linear relationship allows for a direct estimation of the spectral impact on a monthly or annual basis. The linear relation between the $SMM_{monthly}$ and $APE_{monthly}$ also allows calculating the value of SMM_{annual} directly from APE_{annual}, thus revealing that the spectral effects on PV performance for the studied PV technologies would require only the spectral information represented by the weighted *APE*. As publically accessible online databases with experimental and synthetic spectral information, such as the National Solar Radiation Database, become more available, relying on weighted *APE* instead of complete spectral data would significantly reduce costs and computational resources to estimate the spectral performance impact.

Finally, the two indicators, *SAUF* and *SEF* can be used as reasonable estimates for IUF/IUF^{*} and the irradiance-weighted *SMM*, respectively. As alternative indicators, the *SAUF* and *SEF* require only averaged spectra and can, thus, reduce the computational effort to estimate the IUF/IUF^{*} and the irradiance-weighted *SMM*.

Declaration of Competing Interest

The authors declare that they have no known competing financial interests or personal relationships that could have appeared to influence the work reported in this paper.

Acknowledgments

The authors thank the PV-group at the Department of Engineering Sciences, University of Agder, Norway, for providing us with their spectral data for this work. The Peruvian part of this work received financial support from PROCIENCIA and The World Bank through contract 013-2020-FONDECYT-BM. J. A. Töfflinger acknowledges the financial support from the Academic Office of Institutional Affairs and the Vicechancellorship for Research (PI0936) of the Pontificia Universidad Católica del Perú. M. A. Sevillano-Bendezú acknowledges the doctoral scholarship of CONCYTEC through PROCIENCIA, contract N°236-2015-FONDECYT and the financial support "Ayudas de la EDUJA para la realización de tesis doctorales en régimen de cotutela internacional" granted by the University of Jaen. G. Nofuentes sincerely thanks the financial support provided by the Spanish Science and Innovation Ministry and the ERDF within the frame of the project 'Estimación de la energía generada por módulos fotovoltaicos de capa delgada: influencia del espectro' under expedient code ENE2008-05098/ALT. C. Ulbrich acknowledges support by the Initiative and Networking Fund of the Helmholtz Association in the future topic "Energy Systems Integration" under grant number ZT-0002. M. A. Sevillano-Bendezú also thanks Pedro Palacios Ávila for his input during discussions for optimizing some calculations and Julian Mejia Cordero's input during discussions on mathematical issues.

Appendix A. Supplementary data

Supplementary data to this article can be found online at https://doi.org/10.1016/j.solener.2023.04.067.

References

[1] Irena, 2022. World Energy Transitions Outlook 2022: 1.5°C Pathway. (Abu Dhabi).
[2] Irena, 2022. Renewable capacity statistics 2022. (Abu Dhabi).
[3] Belluardo, G., Ingenhoven, P., Sparber, W., Wagner, J., Weihs, P., Moser, D., 2015. Novel method for the improvement in the evaluation of outdoor performance loss rate in different PV technologies and comparison with two other methods. Sol. Energy 117, 139–152.
[4] Moser, D., Del Buono, M., Jahn, U., Herz, M., Richter, M., De Brabandere, K., 2017. Identification of technical risks in the photovoltaic value chain and quantification of the economic impact. Prog. Photovolt. Res. Appl. 25, 592–604.
[5] International Energy Agency 2020 *Report IEA-PVPS T13-18:2020 Uncertainties in Yield Assessments and PV LCOE*.
[6] International Energy Agency 2020 *Report IEA-PVPS T13-20:2020 Climatic Rating of Photovoltaic Task 13 Performance, Operation and Reliability of Photovoltaic Systems*.
[7] Schweiger, M., Herrmann, W., 2015. Energy Rating Label for PV Modules for Improving Energy Yield Prediction in Different Climates *31st Eur*. Photovolt. Sol. Energy Conf. Exhib. 1888–92.
[8] Schweiger, M., Herrmann, W., 2015 Comparison of energy yield data of fifteen PV module technologies operating in four different climates. *2015 IEEE 42nd Photovoltaic Specialist Conference (PVSC) (IEEE)* pp 1–6.
[9] Ruben Vogt, M., Riechelmann, S., Gracia-Amillo, A.M., Driesse, A., Kokka, A., Maham, K., Karha, P., Kenny, R., Schinke, C., Bothe, K., Blakesley, J., Music, E., Plag, F., Friesen, G., Corbellini, G., Riedel-Lyngskar, N., Valckenborg, R., Schweiger, M., Herrmann, W., 2022. PV Module Energy Rating Standard IEC 61853–3 Intercomparison and Best Practice Guidelines for Implementation and Validation. IEEE J. Photovolt. 12, 844–852.
[10] Blakesley, J.C., Huld, T., Müllejans, H., Gracia-Amillo, A., Friesen, G., Betts, T.R., Hermann, W., 2020. Accuracy, cost and sensitivity analysis of PV energy rating. Sol. Energy 203, 91–100.
[11] Kinsey, G.S., Riedel-Lyngskær, N.C., Miguel, A.-A., Boyd, M., Braga, M., Shou, C., Cordero, R.R., Duck, B.C., Fell, C.J., Feron, S., Georghiou, G.E., Habryl, N., John, J. J., Ketjoy, N., López, G., Louwen, A., Maweza, E.L., Minemoto, T., Mittal, A., Molto, C., Neves, G., Garrido, G.N., Norton, M., Paudyal, B.R., Pereira, E.B., Poissant, Y., Pratt, L., Shen, Q., Reindl, T., Rennhofer, M., Rodríguez-Gallegos, C. D., Rüther, R., van Sark, W., Sevillano-Bendezú, M.A., Seigneur, H., Tejero, J.A., Theristis, M., Töfflinger, J.A., Ulbrich, C., Vilela, W.A., Xia, X., Yamasoe, M.A., 2022. Impact of measured spectrum variation on solar photovoltaic efficiencies worldwide. Renew. Energy 196, 995–1016.
[12] Chantana, J., Imai, Y., Kawano, Y., Hishikawa, Y., Nishioka, K., Minemoto, T., 2020. Impact of average photon energy on spectral gain and loss of various-type PV technologies at different locations. Renew. Energy 145, 1317–1324.
[13] Sharma, M.K., Bhattacharya, J., 2022. Dependence of spectral factor on angle of incidence for monocrystalline silicon based photovoltaic solar panel. Renew. Energy 184, 820–829.
[14] Dirnberger, D., Blackburn, G., Müller, B., Reise, C., 2015. On the impact of solar spectral irradiance on the yield of different PV technologies *Sol*. Energy Mater. Sol. Cells 132, 431–442.
[15] Dirnberger, D., Müller, B., Reise, C., 2015. On the uncertainty of energetic impact on the yield of different PV technologies due to varying spectral irradiance. Sol. Energy 111, 82–96.
[16] Sengupta, M., Xie, Y., Lopez, A., Habte, A., Maclaurin, G., Shelby, J., 2018. The National Solar Radiation Data Base (NSRDB). Renew. Sustain. Energy Rev. 89, 51–60.
[17] Xie, Y., Sengupta, M., 2018. A Fast All-sky Radiation Model for Solar applications with Narrowband Irradiances on Tilted surfaces (FARMS-NIT): Part I. The clear-sky model. Sol. Energy 174, 691–702.
[18] Xie, Y., Sengupta, M., Wang, C., 2019. A Fast All-sky Radiation Model for Solar applications with Narrowband Irradiances on Tilted surfaces (FARMS-NIT): Part II. The cloudy-sky model. Sol. Energy 188, 799–812.
[19] Kinsey, G.S., 2021. Solar cell efficiency divergence due to operating spectrum variation. Sol. Energy 217, 49–57.
[20] Xie, Y., Habte, A., Sengupta, M., Vignola, F., 2021. An Evaluation of the Spectral Irradiance Data from the NSRDB. Golden, CO (United States).
[21] Minemoto, T., Nakada, Y., Takahashi, H., Takakura, H., 2009. Uniqueness verification of solar spectrum index of average photon energy for evaluating outdoor performance of photovoltaic modules. Sol. Energy 83, 1294–1299.
[22] Paudyal, B.R., Imenes, A.G., 2021. Uniqueness verification of blue fraction as a parameter of spectral irradiance. quantification 2563–2568.
[23] Rodrigo, P.M., Fernández, E.F., Almonacid, F.M., Pérez-Higueras, P.J., 2017. Quantification of the spectral coupling of atmosphere and photovoltaic system performance: Indexes, methods and impact on energy harvesting. Sol. Energy Mater. Sol. Cells 163, 73–90.
[24] Rodrigo, P.M., Varona, J., Soria-Moya, A., Almonacid-Cruz, B., Fernández, E.F., 2019. Comparative assessment of simplified indexes for the spectral characterisation of photovoltaic systems. Meas. J. Int. Meas. Confed. 133, 1–8.

[25] Louwen, A., De Waal, A.C., Van Sark, W.G.J.H.M., 2017. Evaluation of different indicators for representing solar spectral variation. 2017 IEEE 44th Photovolt Spec. Conf. PVSC 2017, 1–5.
[26] Alonso-Abella, M., Chenlo, F., Nofuentes, G., Torres-Ramírez, M., 2014. Analysis of spectral effects on the energy yield of different PV (photovoltaic) technologies: The case of four specific sites. Energy 67, 435–443.
[27] IEC 2008 *IEC 60904-7 Edition 3.0 Part 7: Computation of the spectral mismatch correction for measurements of photovoltaic devices*.
[28] Ishii, T., Otani, K., Itagaki, A., Utsunomiya, K., 2013. A simplified methodology for estimating solar spectral influence on photovoltaic energy yield using average photon energy. Energy Sci. Eng. 1, 18–26.
[29] Kataoka, N., Yoshida, S., Ueno, S., Minemoto, T., 2014. Evaluation of solar spectral irradiance distribution using an index from a limited range of the solar spectrum. Curr. Appl. Phys. 14, 731–737.
[30] Chantana, J., Mano, H., Horio, Y., Hishikawa, Y., Minemoto, T., 2017. Spectral mismatch correction factor indicated by average photon energy for precise outdoor performance measurements of different-type photovoltaic modules. Renew. Energy 114, 567–573.
[31] Tsuji, M., Rahman, M.M., Hishikawa, Y., Nishioka, K., Minemoto, T., 2018. Uniqueness verification of solar spectrum obtained from three sites in Japan based on similar index of average photon energy. Sol. Energy 173, 89–96.
[32] Imai, Y., Chantana, J., Kawano, Y., Hishikawa, Y., Minemoto, T., 2019. Description of performance degradation of photovoltaic modules using spectral mismatch correction factor under different irradiance levels. Renew. Energy 141, 444–450.
[33] Takeguchi, K., Nakayama, K., Chantana, J., Kawano, Y., Nishimura, T., Hishikawa, Y., Minemoto, T., 2021. Spectral gain and loss of different-type photovoltaic modules through average photon energy of various locations in Japan. Sol. Energy 214, 1–10.
[34] Takeguchi, K., Chantana, J., Kawano, Y., Nishimura, T., Minemoto, T., 2022. Gaussian distribution of average photon energy and spectral gain and loss of several-type photovoltaic modules at different outdoor sites around the world. Opt. Commun. 505, 127516.
[35] Nofuentes, G., García-Domingo, B., Muñoz, J.V., Chenlo, F., 2014. Analysis of the dependence of the spectral factor of some PV technologies on the solar spectrum distribution. Appl. Energy 113, 302–309.
[36] Nofuentes, G., Gueymard, C.A., Aguilera, J., Pérez-Godoy, M.D., Charte, F., 2017. Is the average photon energy a unique characteristic of the spectral distribution of global irradiance? Sol. Energy 149, 32–43.
[37] Neves, G., Vilela, W., Pereira, E., Yamasoe, M., Nofuentes, G., 2021. Spectral impact on PV in low-latitude sites: The case of southeastern Brazil. Renew. Energy 164, 1306–1319.
[38] Ascencio-Vásquez, J., Brecl, K., Topič, M., 2019. Methodology of Köppen-Geiger-Photovoltaic climate classification and implications to worldwide mapping of PV system performance. Sol. Energy 191, 672–685.
[39] Ascencio Vasquez J 2019 Data for: Methodology of Köppen-Geiger-Photovoltaic climate classification and implications to Worldwide Mapping of PV System Performance.
[40] Paudyal, B.R., Somasundaram, S.G., Louwen, A., Reinders, A.H.M.E., van Sark, W. G.J.H.M., Stellbogen, D., Ulbrich, C., Imenes, A.G., 2022. Analysis of spectral irradiance variation in northern Europe using average photon energy as a single parameter. Sol. Energy (Submitted).
[41] Paudyal, B.R., Imenes, A.G. 2020 Analysis of spectral irradiance distribution for PV applications at high latitude *2020 47th IEEE Photovoltaic Specialists Conference (PVSC)* vol 2020-June (IEEE) pp 1834–41.
[42] Driesse, A., Stein, J.S.. Global normal spectral irradiance in Albuquerque: a one-year open dataset for PV research, SAND2020-12693. https://pvpmc.sandia.gov/download/7984/.
[43] Boyd, M., Chen, T., Dougherty, B., n.d. NIST Campus Photovoltaic (PV) Arrays and Weather Station Data Sets. National Institute of Standards and Technology. U.S. Department of Commerce, Washington, D.C. https://doi.org/10.18434/M3S67G.
[44] Solar Radiation Monitoring Laboratory Univ. Oregon (SRML) Spectral Data http://solardat.uoregon.edu/.
[45] Andreas A and Stoffel T 1981 NREL Solar Radiation Research Laboratory (SRRL): Baseline Measurement System (BMS); Golden, Colorado (Data); NREL Report No. DA-5500-56488. https://midcdmz.nrel.gov/apps/sitehome.pl?site=BMS.
[46] Tatsiankou, V., Hinzer, K., Schriemer, H., Kazadzis, S., Kouremeti, N., Gröbner, J., Beal, R., 2018. Extensive validation of solar spectral irradiance meters at the World Radiation Center. Sol. Energy 166, 80–89.
[47] Martín, N., Ruiz, J.M., 1999. A new method for the spectral characterisation of PV modules. Prog Photovolt. Res. Appl. 7, 299–310.
[48] Nofuentes, G., de la Casa, J., Solís-Alemán, E.M., Fernández, E.F., 2017. Spectral impact on PV performance in mid-latitude sunny inland sites: Experimental vs. modelled results. Energy 141, 1857–1868.
[49] Caballero, J.A., Fernandez, E.F., Theristis, M., Almonacid, F., Nofuentes, G., 2018. Spectral Corrections Based on Air Mass, Aerosol Optical Depth, and Precipitable Water for PV Performance Modeling. IEEE J. Photovolt. 8, 552–558.
[50] Micheli, L., Caballero, J.A., Fernandez, E.F., Smestad, G.P., Nofuentes, G., Mallick, T.K., Almonacid, F., 2019. Correlating photovoltaic soiling losses to waveband and single-value transmittance measurements. Energy 180, 376–386.
[51] Conde, L.A., Angulo, J.R., Sevillano-Bendezú, M.Á., Nofuentes, G., Töfflinger, J.A., de la Casa, J., 2021. Spectral effects on the energy yield of various photovoltaic technologies in Lima (Peru). Energy 223 120034.
[52] Holmgren, F., Hansen, W.C., A. Mikofski M,, 2018. Pvlib Python: a Python Package for Modeling Solar Energy Systems. J. Open Source Softw. 3, 884.
[53] Herrmann, W., Nixdorf, I., Bonilla Castro, J., 2020. Uncertainty of PV Module Energy Rating Caused by Spectral Effects. 37th Eur Photovolt. Sol. Energy Conf. Exhib. 816–821.
[54] Rau, U., Blank, B., Müller, T.C.M., Kirchartz, T., 2017. Efficiency Potential of Photovoltaic Materials and Devices Unveiled by Detailed-Balance Analysis *Phys. Rev. Appl.* 7, 1–9.
[55] Shockley, W., Queisser, H.J., 1961. Detailed balance limit of efficiency of p-n junction solar cells. J. Appl. Phys. 32, 510–519.
[56] Jardine, C., Betts, T., Gottschlg, R., Infield, D.G., Lane, K., 2002. Influence of spectral effects on the performance of multijunction amorphous silicon cells. 17th Eur. Photovolt. Sol. Energy Conf. 44, 2–5.
[57] Williams, S.R., Betts, T.R., Helf, T., Gottschalg, R., Beyer, H.G., Infield, D.G., Modelling long-term module performance based on realistic reporting conditions with consideration to spectral effects, in: 3rd World Conference onPhotovoltaic Energy Conversion, 2003. Proceedings of, vol. 2, 2003, pp. 1908–1911.
[58] Eke, R., Betts, T.R., Gottschalg, R., 2017. Spectral irradiance effects on the outdoor performance of photovoltaic modules *Renew*. Sustain. Energy Rev. 69, 429–434.
[59] Minemoto, T., Toda, M., Nagae, S., Gotoh, M., Nakajima, A., Yamamoto, K., Takakura, H., Hamakawa, Y., 2007. Effect of spectral irradiance distribution on the outdoor performance of amorphous Si//thin-film crystalline Si stacked photovoltaic modules. Sol. Energy Mater. Sol. Cells 91, 120–122.
[60] Minemoto, T., Nagae, S., Takakura, H., 2007. Impact of spectral irradiance distribution and temperature on the outdoor performance of amorphous Si photovoltaic modules. Sol. Energy Mater. Sol. Cells 91, 919–923.
[61] Nakada, Y., Takahashi, H., Ichida, K., Minemoto, T., Takakura, H., 2010. Influence of clearness index and air mass on sunlight and outdoor performance of photovoltaic modules. Curr. Appl. Phys. 10. S261–S264.
[62] Hyndman, R.J., Athanasopoulos, G., Forecasting: principles and practice, 2nd edition, OTexts: Melbourne, Australia. OTexts.com/fpp2.
[63] Seabold, S., Perktold, J., 2010 Statsmodels: Econometric and Statistical Modeling with Python *Proc. 9th Python Sci. Conf.*
[64] Meydbray, J., Riley, E., Dunn, L., Emery, K., Kurtz, S., 2012. Pyranometers and Reference Cells: Part 2: What Makes the Most Sense for PV Power Plants? PV Mag, 108 – 10.